Interaction of NO_2 with Model NSR Catalysts: Metal Oxide Interaction Controls Initial NO_x Storage Mechanism

Aine Desikusumastuti, Thorsten Staudt, Zhihui Qin, Markus Happel, Mathias Laurin, Yaroslava Lykhach, Shamil Shaikhutdinov, Friedemann Rohr, and Jörg Libuda*

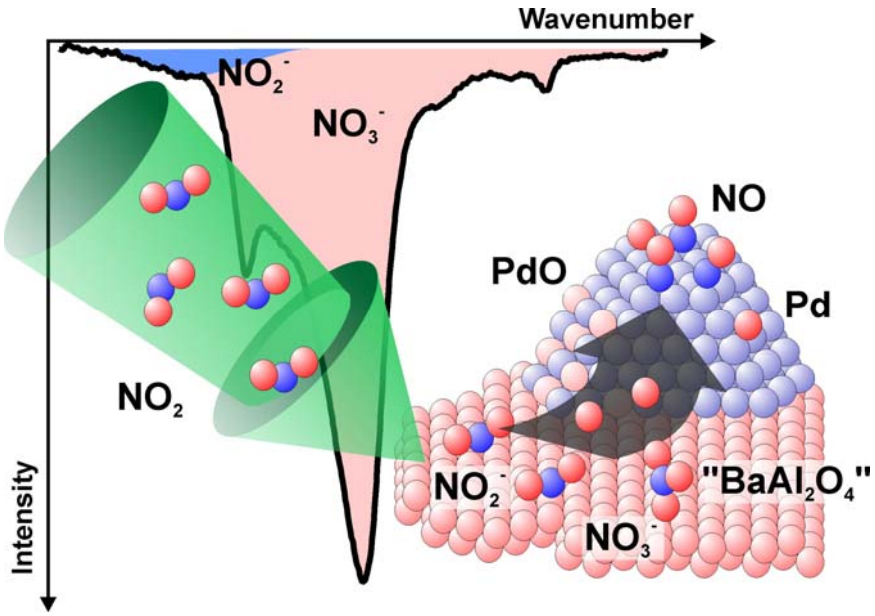

Nitrite formation during the initial stages of NO_x uptake on a nitrogen storage and reduction (NSR) catalyst is critically controlled by the interaction between the barium based NO_x storage material and the supported noble metal nanoparticles. This effect is due to reverse spillover of activated oxygen species, as demonstrated by molecular beam techniques and time-resolved IR surface spectroscopy on a NSR model catalyst.

* Prof. Dr. Jörg Libuda, Lehrstuhl für Physikalische Chemie II, Universität Erlangen-Nürnberg, Egerlandstr. 3, 91058 Erlangen, Germany, FAX: (+49) 9131 8427308; Email: libuda@chemie.uni-erlangen.de;
Aine Desikusumastuti (M. Sc.), Thorsten Staudt (Dipl. Phys.), Markus Happel, Dr. Yaroslava Lykhach, Lehrstuhl für Physikalische Chemie II, Universität Erlangen-Nürnberg, Egerlandstr. 3, 91058 Erlangen; Dr. Mathias Laurin, Lehrstuhl für Physikalsiche Chemie II, Universität Erlangen-Nürnberg, present address: Research Centre for Spectrochemistry, The University of Tokyo, Hongo, Tokyo 113-0033, Japan; Dr. Zhihui Qin, Dr. S. Shaikhutdinov, Fritz-Haber-Institut der Max-Planck-Gesellschaft, Faradayweg 4-6, 14195 Berlin, Germany; Dr. Friedemann Rohr, Umicore AG & Co. KG, Automotive Catalysts, Rodenbacher Chaussee 4, 63403 Hanau-Wolfgang.

Interaction of NO_2 with Model NSR Catalysts: Metal Oxide Interaction Controls Initial NO_x Storage Mechanism

Aine Desikusumastuti, Thorsten Staudt, Zhihui Qin, Markus Happel, Mathias Laurin, Yaroslava Lykhach, Shamil Shaikhutdinov, Friedemann Rohr, and Jörg Libuda*

Abstract

Combining scanning tunneling microscopy (STM), molecular beam (MB) methods and time-resolved infrared reflection absorption spectroscopy (TR-IRAS), we have investigated the mechanism of initial NO_x uptake on a model nitrogen storage and reduction (NSR) catalyst. The model system is prepared by co-deposition of Pd metal particles and Ba containing oxide particles onto an ordered alumina film on NiAl(110). It is shown that the metal oxide interaction between the active noble metal particles and the NO_x storage compound in NSR model catalysts plays an important role in the reaction mechanism. We suggest that strong interaction facilitates reverse-spillover of activated oxygen species from the NO_x storage compound to the metal. The process leads to partial oxidation of the metal nanoparticles and simultaneous stabilization of the surface nitrite intermediate.

Keywords:

Heterogeneous catalysis, Model catalysis, STM, IR, Molecular Beams

* Prof. Dr. Jörg Libuda, Lehrstuhl für Physikalische Chemie II, Universität Erlangen-Nürnberg, Egerlandstr. 3, 91058 Erlangen, Germany, FAX: (+49) 9131 8427308; Email: libuda@chemie.uni-erlangen.de;
Aine Desikusumastuti (M. Sc.), Thorsten Staudt (Dipl. Phys.), Markus Happel, Dr. Yaroslava Lykhach, Lehrstuhl für Physikalische Chemie II, Universität Erlangen-Nürnberg, Egerlandstr. 3, 91058 Erlangen; Dr. Mathias Laurin, Lehrstuhl für Physikalsiche Chemie II, Universität Erlangen-Nürnberg, present address: Research Centre for Spectrochemistry, The University of Tokyo, Hongo, Tokyo 113-0033, Japan; Dr. Zhihui Qin, Dr. S. Shaikhutdinov, Fritz-Haber-Institut der Max-Planck-Gesellschaft, Faradayweg 4-6, 14195 Berlin, Germany; Dr. Friedemann Rohr, Umicore AG & Co. KG, Automotive Catalysts, Rodenbacher Chaussee 4, 63403 Hanau-Wolfgang.

Introduction

Improving fuel and CO_2 efficiency is among the key challenges in future transportation. However, highly fuel-efficient combustion engines, both diesel and lean-burn gasoline, involve operation under lean conditions, i.e. with high air to fuel ratios. Unfortunately, catalytic removal of toxic components such as NO_x turns out to be a severe problem in the strongly oxidizing environment of the resulting exhaust stream. The reason is that efficient operation of classical three-way catalysts is largely limited to a small window around stoichiometric combustions conditions.[1]

Currently, there are two competing concepts which allow NO_x reduction under lean conditions,[2] both of which have been commercialized in passenger cars, recently: selective catalytic reduction (SCR) is based on the reduction of NO_x with ammonia, which is generated onboard by decomposition of urea. The alternative is the so-called NO_x storage and reduction (NSR) catalyst, which is based on the idea that, if NO_x cannot be efficiently reduced during lean operation periods, it may at least be stored by conversion to non-volatile compounds.[3, 4] Typically, Ba containing storage materials are used leading to the formation of $Ba(NO_3)_2$. Once the storage capacity is exceeded, NO_x may be released and reduced during short fuel-rich operation cycles.

Both alternatives, SCR and NSR are linked to characteristic advantages and shortcomings. An SCR system performs well under high temperature and high NO_x feed conditions. The fuel economy is usually slightly better than in the NSR case since no rich operation is necessary. The low temperature performance on the other hand, especially with high NO/NO_2 ratios in the feedgas is a concern for SCR systems. While SCR catalysts are precious metal free, the necessary infrastructure comprising urea tank and dosing system is costly. Other issues associated with SCR systems is the availability of urea and compliance. Due to the high NO_x-engine out emissions for lean-burn gasoline applications, SCR is momentarily only an option in diesel applications. The NSR concept, in the other hand, is a stand-alone solution that does not require a secondary reducing agent. While conversions at high temperatures and NO_x loads are limited, moderate conversions under relevant driving conditions can be achieved. Since an NSR contains basic components, it tends to be sensitive to sulfur poisoning and needs to be desulfated in regular intervals. There is a small fuel penalty of some 2% linked to the rich events for regenerating the NSR and for sulfur removal. For lighter passenger cars the NSR is quite cost-competitive and there exists a number of NSR equipped applications, both diesel and lean-burn gasoline.[5, 6]

Since the NSR concept was suggested by Toyota in 1996,[3] there has been a large number of studies on this topic in applied catalysis.(see e.g. [4, 7-14] and references therein) Nevertheless, little insight was obtained into the mechanism and microkinetics of the NO_x storage and release process at the microscopic scale. The reason is that both materials and reaction mechanisms are outstandingly complex. Especially, the fundamental mechanism of the initial storage process is

currently under debate. Whereas several experimental studies point to a sequential formation of nitrites and nitrates ([9, 15-18], compare also [4]), theoretical calculations[19-22] and few recent experimental studies[23, 24] suggest initial formation of nitrite-nitrate pairs. Detailed insights into these mechanistic issues may potentially open up routes towards a more rational improvement of the NSR concept.

Such molecular-level insights may be provided by mechanistic and microkinetic studies on well-defined model catalysts.[16, 25-31] Surprisingly, there have been very few attempts to translate the NSR concept to a tractable model approach. Pioneering work on the interaction of NO_2 with model BaO surfaces has been published by Bowker and coworkers,[16, 32, 33] Szanyi and coworkers[23, 34-37] and recently by our group.[18, 38-40] Here, we present the first model study on a "complete" NSR model system, involving the Ba storage compound and co-deposited noble metal nanoparticles on an alumina model support. By taking advantage of the full spectrum of surface-science methods, the structural and chemical properties of the model system is characterized and the degree of metal oxide interaction controlled in great detail. Combining this information with time-resolved infrared reflection absorption spectroscopy (TR-IRAS) (see e.g. [26, 41]) and molecular beam (MB) methods (see e.g. [26, 42, 43]), we provide evidence for a reaction mechanism which may help to explain the contradicting results in the literature: we show that the initial storage mechanism is directly linked to the interaction of the storage compound with the supported metal nanoparticles. This interaction facilitates reverse-spillover of activated oxygen species, resulting in partial oxidation of the noble metal nanoparticles and simultaneous stabilization of surface nitrites on the NO_x storage compound.

Experimental Part

MB/IRAS experiments were performed in an UHV apparatus at the University Erlangen-Nuremberg, which allows up to four effusive beams and a supersonic beam to be superimposed on the sample. Additionally, the system is equipped with a FTIR spectrometer (Bruker IFS66/v), a beam monitor which allows alignment and intensity calibration of the beams, two quadrupole mass spectrometers, a vacuum transfer system with high pressure cell and all necessary preparation tools. The NO_2 beam (Linde, 99.0%) was generated from an effusive beam doser and modulated by a valve system. All measurements were performed by remote controlled sequences, exposing the sample to pulses of NO_2 at variable beam intensities between 1.6×10^{13} $cm^{-2}s^{-1}$ (equivalent pressure: 0.7×10^{-7} mbar) and 3.2×10^{15} $cm^{-2}s^{-1}$ (equivalent pressure 1.4×10^{-5} mbar), followed by acquisition of IR spectra. IR spectra were acquired at a spectral resolution of 2 cm^{-1} with typical acquisition times of 118 s.

STM measurements (Micro H, Omicron) were performed in a separate UHV chamber at the Fritz-Haber-Institute, Berlin). The chamber is equipped with standard sample cleaning/preparation facilities. All images were recorded using commercial Pt/Ir tips (L.O.T.-Oriel GmbH) with tunneling parameters (bias and current) as follows: Fig. 1, A: +3.0V, 0.15nA; B: +2.7V, 0.16nA; C: +2,6V, 0.16nA; D: +2.2V, 0.17nA; E: +2.5V, 0.17nA; F: +2.8V, 0.15nA.

For preparation of the model surfaces, a NiAl(110) surface was cleaned by numereous cycles of sputtering and vacuum annealing, followed by two cycles of oxidation in 10^{-6} mbar O_2 at 550 K and UHV annealing at 1135 K in order to prepare the Al_2O_3 film on NiAl(110). With respect to the details of the procedure we refer to the literature.[44] The quality of the film was checked by LEED, and complete oxidation of the surface was proven by the absence of CO adsorption at 100 K.

For the preparation of the BaO particles, we proceeded as follows: First, the Ba metal was manually cleaned under inert gas atmosphere (glove box) and placed into a Mo crucible. In order to prevent oxidation, the crucible filled with Ba was covered with decane before it was mounted in a commercial electron beam assisted evaporator (Focus EFM3). The evaporator was installed into the UHV chamber immediately before pumping out. Under UHV conditions, the Ba source was calibrated using a quartz microbalance. During deposition the sample was biased to the same potential as the Ba source in order to avoid surface defect generation by Ba ion bombardment. Ba was deposited at 300 K at typical rates of 4.8×10^{12} atoms$\cdot$cm$^{-2}\cdot$s^{-1} (an average film thickness of 1 Å Ba corresponds to $1.6\text{x}10^{14}$ atoms$\cdot$cm^{-2}).

Pd was deposited using the same type of exaporator (Focus EFM3), but evaporation was performed from a wire (Goodfellow, >99.9%). Typical deposition rates were around 5.7×10^{12} atomcm^{-2}s^{-1} (1 Å Pd corresponds to 6.8×10^{14} atoms$\cdot$cm^{-2}). Again, the sample was biased to avoid ion damage.

For the experiments shown in Fig.1 and 2, 1 Å Ba was deposited prior to deposition of 1 Å Pd, or, vice versa, 1 Å Pd was deposited prior to deposition of 1 Å Ba. In both cases Ba was oxidized immediately after deposition by exposure to 6×10^{-7} mbar O_2 for 90 s. Alternatively, Ba was annealed in 6×10^{-7} mbar O_2 up to 800 K For the experiment in Fig. 3, thicker BaO and Pd layers were used (roughly 20 Å Ba and 4 Å Pd). Oxidation was performed by exposing for 900 s to 6×10^{-7} mbar O_2 and annealing up to 800 K.

Results and Discussion

The preparation of the NSR model system is summarized in Fig. 1, showing selected scanning tunneling microscopy (STM) images of different preparation stages. As a model support, we use an ordered Al_2O_3 thin film, prepared on NiAl(110).[45, 46] The NO_x storage compound is prepared by physical vapor deposition (PVD) of Ba in ultrahigh vacuum (UHV) and subsequent oxidation by O_2 exposure. As shown in a recent high-resolution photoelectron spectroscopy (HR-PES) study using

synchrotron radiation, the procedure yields three dimensional barium aluminate-like ("$BaAl_2O_4$") nanoparticles.[38] The formation of such aluminate phases is well-known, also for real catalyst materials.[47-49] Upon annealing in O_2 to 800 K, the Ba aluminate nanoparticle system is preserved, with the particles showing slow ripening, restructuring and diffusion into the support.

In a second step, Pd is deposited by PVD, either on the annealed or on the non-annealed "$BaAl_2O_4$"/Al_2O_3. We have characterized the Pd/BaO co-deposition system in detail by STM and IRAS and adsorption studies using CO as a probe molecule; a detailed discussion will be provided in a forthcoming publication.[50] Briefly, the findings can be summarized as follows: In contrast to the deposition of Ba, Pd only weakly interacts with Al_2O_3 support and the Pd atoms are more mobile.[51] As a result, the Pd nucleates at the "$BaAl_2O_4$" nanoparticles, efficiently decorating their surface (see Fig. 1e). Now, we can take advantage of this difference in growth behavior, in order to modify the Pd/BaO interaction. This is done by reversing the deposition sequence. Deposition of Pd first leads to formation large Pd nanocrystallites, preferentially nucleation at oxide defects such as domain boundaries (see Fig. 1d). Subsequent deposition of Ba and oxidation generates small Ba containing aggregates on the Al_2O_3 support and at the Pd particles (Fig. 1f). The aggregates on the Pd particles are in intimate contact with the Pd surface, blocking a large fraction of the Pd adsorption sites.[50] It is noteworthy that the IR spectra after NO_2 exposure for this system are very similar to those for Ba deposition directly on the Al_2O_3 support (see below). This suggests that Ba alumiate-like nanoparticles are formed in the case of Ba deposition/oxidation on Pd/Al_2O_3 as well. Future HR-PES experiments may provide more detailed information on the properties and stoichiometry of these aggregates.

In order to probe the effect of the structure and Pd/BaO interaction on the storage mechanism, we utilized the above described selection of model systems and perform systematic IRAS/MB experiments during reaction with NO_2. Selected IR spectra of the NO stretching frequency region for the different NSR model systems and selected NO_2 exposures are displayed in Fig. 2 (1 L (Langmuir) corresponds to a gas dose of 10^{-6} Torr·s). The assignment of the spectral features was discussed in detail in recent publications, making systematic comparisons with density functional theory (DFT) calculations [39] and XPS.[18] Briefly, the feature at 1250 cm^{-1} is assigned to a flat-lying surface nitrite (NO_2^-), the intensity of which is low due to the orientation of the dynamic dipole moment nearly parallel to the surface. The features at 1330 and 1460 cm^{-1} are attributed to bridging and monodentate surface nitrates (NO_3^-), the ratio of which depends on coverage, temperature and particle size.[39] It should be pointed out that IRAS does not facilitate straightforward quantification of the different species, because of dipole coupling effects and varying size and orientation of the dynamic dipoles.[41, 52-54] In particular, this holds for the relative intensity of the nitrite and nitrate bands (compare [39],[18]) However, the qualitative appearance and

disappearance of surface species can be followed easily and the for individual species the band intensity also semi-quantitatively follows the surface concentration (as recently shown in combined XPS/IRAS experiments, see [18]).

By comparison of the spectra in Fig.2, three conclusions may be drawn: First, we observe the formation of surface nitrites (NO_2^-) and surface nitrates (NO_3^-) for all model systems investigated. Secondly, surface nitrites are formed at the initial stage of the reaction (the intensity of the band at 1250 cm^{-1} decreases with increasing NO_2 exposure), whereas at a later stage surface nitrate become the dominating species due to conversion of nitrites into nitrates (increasing intensity of bands at 1330 and 1460 cm^{-1}, see also [18]).

The most important observation relates, however, to the intensity of the nitrite feature at 1250 cm^{-1}, which differs strongly for the model systems investigated. This observation suggests that nitrite formation strongly depends on the properties of the NSR model system with particularly strong nitrite features being observed in the presence of Pd nanoparticles. The strongest signature of a surface nitrite is found for the model system, for which we expect a particularly strong Pd/BaO interaction, i.e. with small "$BaAl_2O_4$" aggregates directly covering the Pd nanoparticles ("$BaAl_2O_4$"/Pd/Al_2O_3, Fig. 2d). Apparently, the Pd/BaO interaction critically controls the degree of surface nitrite formation.

In order to elucidate the mechanistic origin of this effect, we have performed TR-IRAS coupled to MB dosing. The experimental procedure is illustrated in the inset in Fig. 3. NO_2 pulses of different intensity and duration are applied in a remote controlled procedure, followed by acquisition of IR spectra. Using this procedure, the formation and decomposition of reaction intermediates is systematically monitored over a very broad range of NO_2 exposure, spanning over more than five orders of magnitude.

Briefly, the following behavior is found: At low exposure, the sequential appearance of three bands is observed at 1510, 1640 and 1750 cm^{-1}, which gradually blue-shift by 30-50 cm^{-1} with increasing NO_2 dose. These features can be attributed to the dissociation of NO_2 on the Pd Nanoparticles, giving rise to molecularly adsorbed NO and co-adsorbed atomic oxygen. Based on a detailed comparison with DFT calculations, we have recently identified these features as NO adsorbed in threefold hollow sites on Pd(111) facets (~1510 cm^{-1}), bridging NO adsorbed at (111)/(111) particle edges (~1640 cm^{-1}) and on-top-NO adsorbed at particle corners (~1750 cm^{-1}).[55] The sites are subsequently populated and show a blue shift with NO_2 exposure as a result of dipole coupling and co-adsorption with atomic oxygen.

A surprising effect, however, is observed with increasing NO_2 exposure: Between 1 and 10 L NO_2, all Pd derived NO features disappear, simultaneously with the appearance of the surface nitrite feature at 1250 cm^{-1}. The inset in Fig. 3 shows the integral intensity of the N-O stretching bands due

to molecularly adsorbed NO on Pd, surface nitrites (NO_2^-) and surface nitrates (NO_3^-). Apparently, the disappearance of the molecularly adsorbed NO is directly correlated to the appearance of the surface nitrite. Similarly, the appearance of the surface nitrate is related to the disappearance of the surface nitrite. The latter effect has been observed in previous studies and is attributed to the conversion of surface nitrites to nitrates by gas phase NO_2. But how could NO adsorption on the Pd nanoparticles be affected by nitrite formation on the "$BaAl_2O_4$" aggregates?

Apparently we have to invoke that a surface species, generated during nitrite formation on "$BaAl_2O_4$", leads to a modification of the Pd surface. Taking into account that nitrite formation is a redox process involving reduction of NO_2, we may invoke the generation of an activated oxygen species. This species could then interact with Pd, leading to oxygen adsorption on the Pd nanoparticles or surface oxidation. At this point we may refer to recent studies on the oxidation of Pd single crystal surfaces and nanoparticles.[56-59] Under quite moderate conditions, Pd surface oxides are formed on both single crystals and nanoparticles, preceding the formation of bulk PdO.[56-59] Upon transformation to the surface oxide, the interaction with small molecules becomes rather weak,[60-62] which would explain the desorption of molecularly adsorbed NO. In order to rationalize the correlation between Pd oxidation and nitrite formation, we suggest a tentative reaction mechanism as illustrated in Fig. 4: At low NO_2 exposure, NO_2 adsorbs dissociatively on the Pd nanoparticles, leading to a co-adsorption of NO and atomic oxygen. In a slower process, formation of a surface nitrite (NO_2^-) occurs on the "$BaAl_2O_4$" particles. This reaction requires electron transfer from the oxide to the NO_2, resulting is an electron hole within the oxide 2p band. This hole which can be healed via several reaction pathways. One possibility is the theoretically predicted pathway of nitrite-nitrate pair formation. Based on the above observation, we suggest an alternative pathway, which involves reverse-spillover of an activated oxygen species to the Pd nanoparticles. As a result, the process opens up a new pathway to oxidation of the Pd particle surface, overcoming the characteristic kinetic hindrance to oxidation at low temperature (compare [59, 63, 64]). Due to the weak interaction of NO with surface PdO, NO desorbs from the Pd particles in parallel with the process of surface oxidation. After complete oxidation of the Pd particle surface, conversion of the nitrite into nitrate occurs at a low rate via reaction with further molecular NO_2. Here it should be noted that the metal-mediated pathway as described above is certainly not the only possible reaction. Indeed, NO_2 uptake also works in the absence of any noble metal and the reaction products are characterized by similar vibrational spectra [39], [18]. The results show, however, that in the presence of noble metal particle, these are directly involved in the uptake mechanism.

It should be pointed out that the evidence for oxide formation is indirect and, certainly, has to be verified in future studies, for example by time-resolved HR-PES under reaction conditions. Apart from the loss of NO adsorption, however, there is a second indication for the oxidation of the Pd

particles. This evidence is derived from an additional feature in the IRAS spectrum observed at 1550 cm^{-1} (see Fig. 3). This band is not observed on metallic Pd but only appears after complete loss of all chemisorbed NO. It may tentatively be attributed to a surface nitrate species adsorbed on PdO, which can only be formed after surface oxidation. In any case it can be concluded that there is a close correlation between nitrite formation and the loss of NO adsorption capacity on the Pd particles, which strongly suggests that both processes are directly linked.

Conclusions

In summary, we have prepared model NSR catalysts by sequential deposition of Pd and Ba (with subsequent oxidation) onto an ordered Al_2O_3 film on NiAl(110), and characterized these systems by STM. The initial mechanism of NO_2 uptake was investigated using a combination of MB methods and IRAS and was compared to Pd free models. I was shown that the metal oxide interaction between the active noble metal particles and the NO_x storage compound in NSR model catalysts critically controls the reaction mechanism. We suggest that a strong interaction facilitates reverse-spillover of activated oxygen species from the NO_x storage compound to the metal. The process leads to partial oxidation of the metal nanoparticles and simultaneous stabilization of the surface nitrite intermediate. The present findings show that metal-oxide interactions may not only involve structural and electronic modification or spillover of adsorbates, but also redox processes within the supported metal particle itself. Similar mechanisms may be expected to be operative for other supported metal systems and the reverse-spillover mediated pathway may play a crucial role in overcoming kinetic barriers to oxidation of noble metal nanoparticles at low reaction temperatures. The present findings underline the outstanding importance of understanding and controlling metal support interactions in complex, multiply nanostructured catalyst materials.

Acknowledgement

The authors thank Hans-Joachim Freund (FHI Berlin) for supporting the STM measurements. The authors thank Karsten Meyer, Matthias Moll, Marc Gärtner and Carola Vogel (University Erlangen) and Friederike Jentoft and Robert Schlögl (FHI, Berlin) for the possibility to use their local glove box facilities. The authors thank Henrik Grönbeck and Konstantin M. Neyman for fruitful cooperations and discussions. We acknowledge financial support of the DFG within specific projects and within the framework to the Excellence Cluster “Engineering of Advanced Materials” in the framework of the excellence initiative, the DAAD, EU (COST D-41), and the Fonds der Chemischen Industrie.

References

[1] R. M. Heck, R. J. Farrauto, S. T. Gulati, *Catalytic Air Pollution Control - Commercial Technology*, John Wiley & Sons, **2002**.

[2] P. Forzatti, I. Nova, L. Castoldi, *Chemical and Biochemical Engineering Quarterly* **2005**, *19*, 309-323.

[3] N. Takahashi, H. Shinjoh, T. Iijima, T. Suzuki, K. Yamazaki, K. Yokota, H. Suzuki, N. Miyoshi, S. Matsumoto, T. Tanizawa, T. Tanaka, S. Tateishi, K. Kasahara, *Catal. Today* **1996**, *27*, 63.

[4] W. S. Epling, L. E. Campbell, A. Yezerets, N. W. Currier, J. E. Parks II, *Catalysis Reviews* **2004**, *46*, 163.

[5] J. Schommers, C. Enderle, H. Breitbach, B. Lindemann, M. Stotz, M. Paule, in *15. Aachener Kolloquium Fahrzeug- und Motorentechnik*, **2006**.

[6] U. Göbel, W. Müller, I. Grißtede, F. Rohr, in *29. Internationales Wiener Motorensymposium*, **2008**.

[7] C. Sedlmair, K. Seshan, A. Jentys, J. A. Lercher, *J. Catal.* **2003**, *214*, 308.

[8] B. Westerberg, E. Fridell, *J. Mol. Catal. A - Chemical* **2001**, *165*, 249.

[9] I. Nova, L. Castoldi, F. Prinetto, V. DalSanto, L. Lietti, E. Tronconi, P. Forzatti, G. Ghiotti, R. Psaro, S. Recchia, *Top. Catal.* **2004**, *30/31*, 181.

[10] M. Piacentini, R. Stroebel, M. Maciejewski, S. E. Pratsinis, A. Baiker, *J. Catal.* **2006**, *243*, 43.

[11] F. Rohr, S. D. Peter, E. Lox, M. Kögel, A. Sassi, L. Juste, C. Rigaudeau, G. Belot, P. Gelin, M. Primet, *Appl. Catal. B - Environmental* **2005**, *56*, 201.

[12] L. Castoldi, R. Matarrese, L. Lietti, P. Forzatti, *Appl. Catal. B: Environ.* **2006**, *64*, 25.

[13] R. G. Tonkyn, R. S. Disselkamp, C. H. F. Peden, *Catal. Today* **2006**, *114*, 94.

[14] J. Dawody, I. Tonnies, E. Fridell, M. Skoglundh, *Top. Catal.* **2007**, *42-43*, 183.

[15] P. J. Schmitz, R. J. Baird, *J. Phys. Chem. B* **2002**, *106*, 4172.

[16] A. Tsami, F. Grillo, M. Bowker, R. M. Nix, *Surf. Sci.* **2006**, *600*, 3403.

[17] C. Hess, J. H. Lunsford, *J. Phys. Chem. B* **2002**, *106*, 6358.

[18] A. Desikusumastuti, M. Happel, K. Dumbuya, T. Staudt, M. Gottfried, H.-P. Steinrück, J. Libuda, *J. Phys. Chem. C* **2008**, *112*, 6477.

[19] P. Broqvist, H. Grönbeck, E. Fridell, I. Panas, *J. Phys. Chem. B* **2004**, *108*, 3523.

[20] H. Grönbeck, P. Broquist, I. Panas, *Surf. Sci.* **2006**, *600*, 403.

[21] W. F. Schneider, K. C. Hass, M. Miletic, J. L. Gland, *J. Phys. Chem B* **2002**, *106*, 7405.

[22] M. Miletic, J. L. Gland, K. C. Hass, W. F. Schneider, *J. Phys. Chem. B* **2003**, *107*, 157.

[23] C.-W. Yi, J. H. Kwak, J. Szanyi, *J. Phys. Chem C* **2007**, *111*, 15299.

[24] A. Desikusumastuti, T. Staudt, M. Happel, M. Laurin, J. Libuda, **submitted**.

[25] J. Libuda, *ChemPhysChem* **2004**, *5*, 625.

[26] J. Libuda, H.-J. Freund, *Surf. Sci. Rep.* **2005**, *57*, 157.

[27] M. S. Chen, D. W. Goodman, *Acc. Chem. Res.* **2006**, *39*, 739.

[28] C. R. Henry, *Surf. Sci. Rep.* **1998**, *31*, 231.

[29] K. Judai, S. Abbet, A. S. Worz, U. Heiz, C. R. Henry, *J. Am. Chem. Soc.* **2004**, *126*, 2732.

[30] S. L. Tait, Z. Dohnalek, C. T. Campbell, B. D. Kay, *Surf. Sci.* **2005**, *591*, 90.

[31] T. Nowitzki, A. F. Carlsson, O. Martyanov, M. Naschitzki, V. Zielasek, T. Risse, M. Schmal, H.-J. Freund, M. Bäumer, *J. Phys. Chem C* **2007**, *111*, 8566.

[32] M. Bowker, M. Cristofolini, M. Hall, E. Fourre, F. Grillo, E. McCormack, P. Stone, M. Ishii, *Top. Catal.* **2007**, *42-34*, 341.

[33] P. Stone, M. Ishii, M. Bowker, *Surf. Sci.* **2003**, *537*, 179.

[34] C.-W. Yi, J. H. Kwak, C. H. F. Peden, H. Wang, J. Szanyi, *J. Phys. Chem C* **2007**, *111*, 14942.

[35] E. Ozensoy, C. H. F. Peden, J. Szanyi, *J. Phys. Chem B* **2006**, *110*, 17001.

[36] E. Ozensoy, C. H. F. Peden, J. Szanyi, *J. Phys. Chem B* **2006**, *110*, 17009.

[37] E. Ozensoy, C. H. F. Peden, J. Szanyi, *J. Phys. Chem B* **2006**, *110*, 8025.

[38] T. Staudt, A. Desikusumastuti, M. Happel, E. Vesselli, A. Baraldi, S. Gardonio, S. Lizzit, F. Rohr, J. Libuda, *J. Phys. Chem C* **2008**, *in press*.

[39] A. Desikusumastuti, T. Staudt, H. Grönbeck, J. Libuda, *J. Catal.* **2008**, *255*, 127.

[40] A. Desikusumastuti, M. Laurin, M. Happel, Z. Qin, S. Shaikhutdinov, J. Libuda, *Catal. Lett.* **2008**, *121*, 311.

[41] J. Libuda, *Surf. Sci.* **2005**, *587*, 55.

[42] G. Scoles, *Atomic and Molecular Beam Methods*, Oxford University Press, Oxford, **1988**.

[43] A. W. Kleyn, *Chem. Soc. Rev.* **2003**, *32*, 87.

[44] R. M. Jaeger, H. Kuhlenbeck, H.-J. Freund, M. Wuttig, W. Hoffmann, R. Franchy, H. Ibach, *Surf. Sci.* **1991**, *259*, 235.

[45] J. Libuda, F. Winkelmann, M. Bäumer, H.-J. Freund, T. Bertrams, H. Neddermeyer, K. Müller, *Surf. Sci.* **1994**, *318*, 61.

[46] G. Kresse, M. Schmid, E. Napetschnig, M. Shishkin, L. Köhler, P. Varga, *Science* **2005**, *308*, 1440.

[47] D. H. Kim, J. H. Kwak, J. Szanyi, S. D. Burton, C. H. F. Peden, *Appl. Catal. B: Environ.* **2007**, *72*, 233.

[48] M. Casapu, J.-D. Grunwaldt, M. Maciejewski, A. Baiker, M. Wittrock, U. Göbel, S. Eckhoff, *Top. Catal.* **2007**, *42-43*, 3.

[49] M. Casapu, J.-D. Grunwaldt, M. Macielewski, M. Wittrock, U. Göbel, A. Baiker, *Appl. Catal. B: Environ.* **2006**, *63*, 232.

[50] A. Desikusumastuti, Z. Qin, T. Staudt, M. Happel, M. Laurin, Y. Lykhach, S. Shaikhutdinov, J. Libuda, **unpublished**.

[51] M. Bäumer, H.-J. Freund, *Prog. Surf. Sci.* **1999**, *61*, 127.

[52] F. M. Hoffmann, *Surf. Sci. Rep.* **1983**, *3*, 107.

[53] P. Hollins, *Surf. Sci. Rep.* **1992**, *16*, 51.

[54] S. Schauermann, J. Hoffmann, V. Johánek, J. Hartmann, J. Libuda, H.-J. Freund, *Angew. Chem. Int. Ed.* **2002**, *41*, 2532.

[55] F. Vines, A. Desikusumastuti, T. Staudt, A. Görling, J. Libuda, K. M. Neyman, *J. Phys. Chem. C* **2008**, *in press*.

[56] M. Todorova, E. Lundgren, V. Blum, A. Mikkelsen, S. Gray, J. Gustafson, M. Borg, J. Rogal, K. Reuter, J. N. Andersen, M. Scheffler, *Surf. Sci.* **2003**, *541*, 101.

[57] E. Lundgren, G. Kresse, C. Klein, M. Borg, J. N. Andersen, M. De Santis, Y. Gauthier, C. Konvicka, M. Schmid, P. Varga, *Phys. Rev. Lett.* **2002**, *88*, 246103.

[58] T. Schalow, M. Laurin, B. Brandt, S. Schauermann, S. Guimond, H. Kuhlenbeck, D. E. Starr, S. k. Shaikhutdinov, J. Libuda, H.-J. Freund, *Angew. Chem. Int. Ed.* **2005**, *44*, 7601.

[59] T. Schalow, B. Brandt, D. E. Starr, M. Laurin, S. K. Shaikhutdinov, S. Schauermann, J. Libuda, H.-J. Freund, *Angew. Chem. Int. Ed.* **2006**, *45*, 3775.

[60] T. Schalow, B. Brandt, D. E. Starr, M. Laurin, S. Schauermann, S. K. Shaikhutdinov, J. Libuda, H.-J. Freund, *Catal. Lett.* **2006**, *107*, 189.

[61] T. Schalow, B. Brandt, D. E. Starr, M. Laurin, S. K. Shaikhutdinov, S. Schauermann, J. Libuda, H.-J. Freund, *Phys. Chem. Chem. Phys.* **2007**, *9*, 1347.

[62] B. Brandt, T. Schalow, M. Laurin, S. Schauermann, J. Libuda, H.-J. Freund, *J. Phys. Chem. B* **2007**, *111*, 938.

[63] E. Lundgren, J. Gustafson, A. Mikkelsen, J. N. Andersen, A. Stierle, H. Dosch, M. Todorova, J. Rogal, K. Reuter, M. Scheffler, *Phys. Rev. Lett.* **2004**, *92*, 046101.

[64] N. Kasper, A. Stierle, P. Nolte, Y. Jin-Phillipp, T. Wagner, D. G. d. Oteyza, H. Dosch, *Surf. Sci.* **2006**, *600*, 2860.

Figure Captions

Fig. 1: Summary of the preparation and structure of the NSR model catalyst used in this study (all STM images: 100 nm × 100 nm): (a) The support is an atomically flat Al_2O_3 film on NiAl(110). The bright lines in the STM images are oxide domain boundaries; (b) Ba deposition and oxidation results in the formation of small "$BaAl_2O_4$" nanoparticles, which can be stabilized by annealing in oxygen (c). Upon subsequent Pd deposition (e), the Pd particles nucleate at the "$BaAl_2O_4$" aggregates. Pd deposition on the pristine oxide films (d) leads to formation of large Pd nanocrystallites, which are partially covered by "$BaAl_2O_4$" aggregates upon Ba deposition and oxidation. The small spots are "$BaAl_2O_4$" aggregates nucleating on the support. See text for details.

Fig. 2: Comparison of selected IR spectra of different model NSR catalysts after exposure to NO_2 at 300 K (the experimental setup is illustrated in the inset): (a) "$BaAl_2O_4$"/Al_2O_3 without Pd component; (b) Pd deposited on "$BaAl_2O_4$"/Al_2O_3 after annealing in O_2 at 800 K; (c) Pd deposited on "$BaAl_2O_4$"/Al_2O_3 without annealing; (d) "$BaAl_2O_4$"/Pd/Al_2O_3 prepared by deposition of Ba and oxidation onto Pd/Al_2O_3. The metal oxide interaction strength is assumed to increase from (a) to (d). Features in the IR spectra due to the formation of surface nitrites (NO_2^-) and nitrates (NO_3^-) are indicated.

Fig. 3: Time-resolved IR spectroscopy of the Pd/"$BaAl_2O_4$"/Al_2O_3 during exposure to a molecular beam of NO_2. The inset (top) illustrates the experimental procedure. Features assigned to the formation of NO on the Pd nanoparticles, surface nitrites (NO_2^-) and surface nitrates (NO_3^-) are indicated. The inset shows the integral intensity of the corresponding bands in the IR spectra. It is seen that the loss of NO and the of formation of the surface nitrites (NO_2^-) are correlated similar as the formation of surface nitrates (NO_3^-) and the loss of surface nitrites (NO_2^-) at higher NO_2 exposure (see text for discussion).

Fig. 4: Schematic representation of the reaction mechanism controlled by the metal oxide interaction, as suggested in this contribution (see text for discussion).

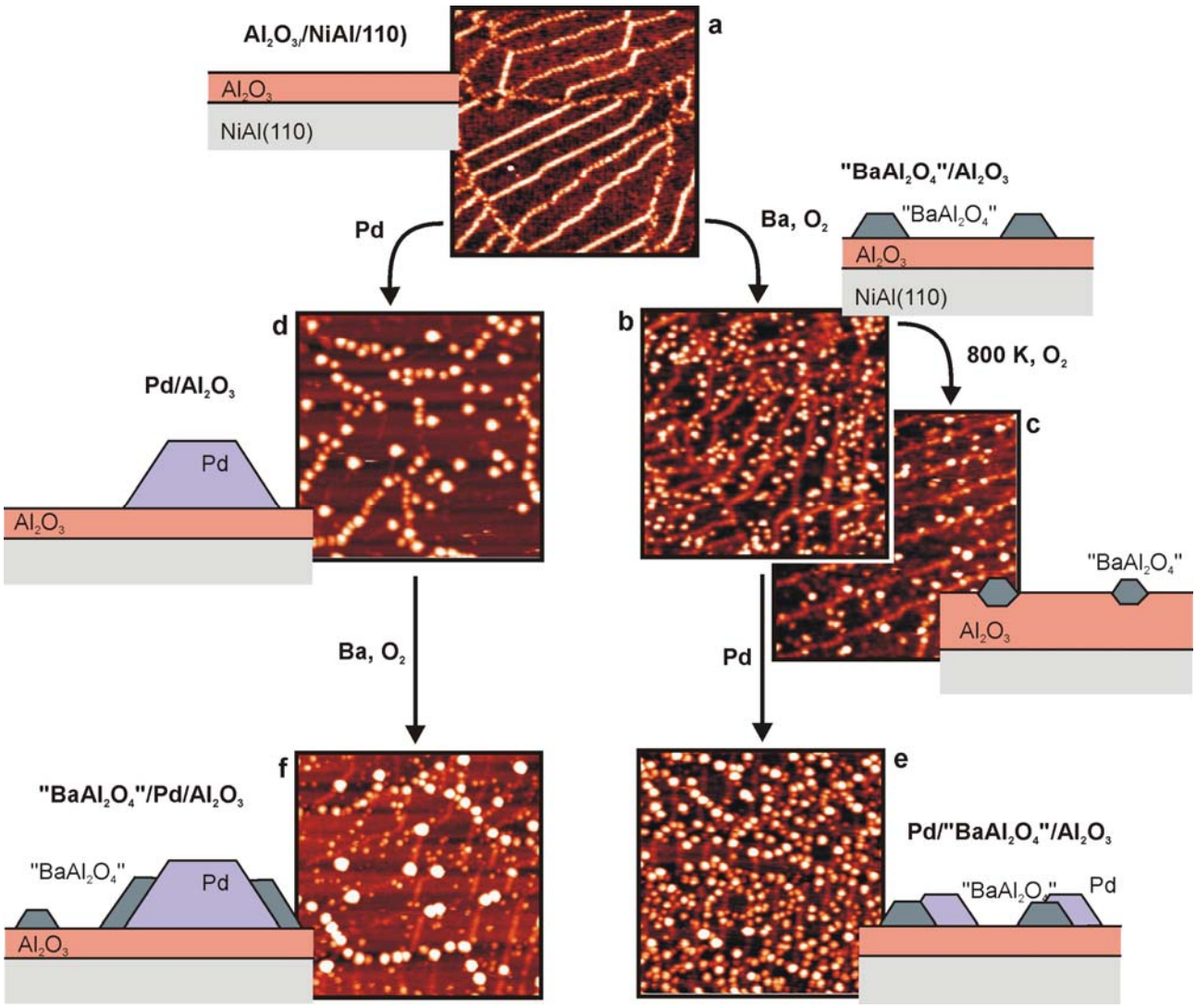
Al2O3/NiAl/110)
a
Al2O3
NiAl(110)
Pd
Ba, O2
"BaAl2O4"/Al2O3
"BaAl2O4"
Al2O3
NiAl(110)
d
b
800 K, O2
Pd/Al2O3
Pd
Al2O3
c
"BaAl2O4"
Al2O3
Ba, O2
Pd
f
e
"BaAl2O4"/Pd/Al2O3
"BaAl2O4"
Pd
Al2O3
Pd/"BaAl2O4"/Al2O3
"BaAl2O4"
Pd

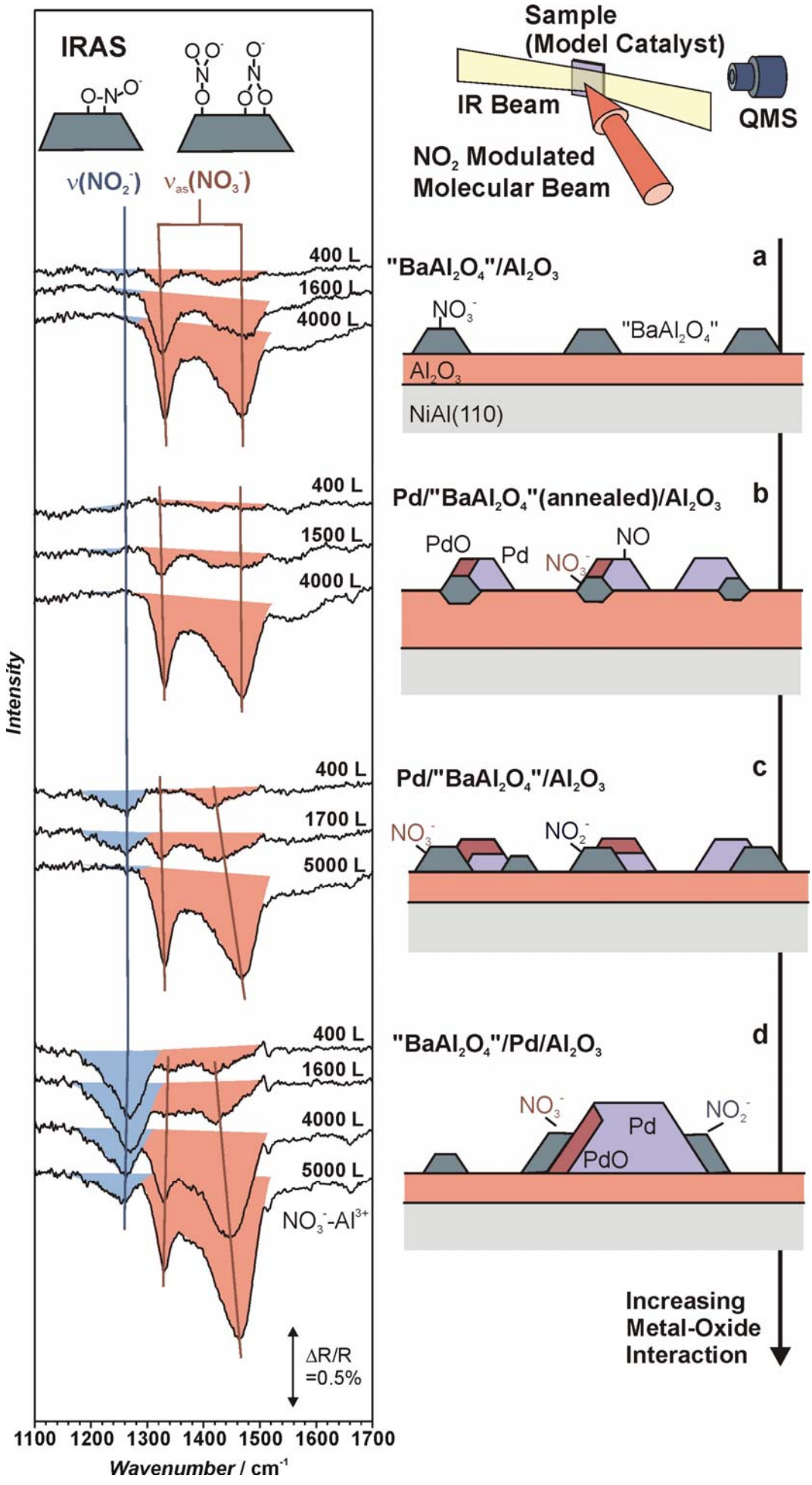
IRAS
ν(NO2-)
νas(NO3-)
400 L
1600 L
4000 L
400 L
1500 L
4000 L
400 L
1700 L
5000 L
400 L
1600 L
4000 L
5000 L
NO3--Al3+
ΔR/R
=0.5%
Intensity
1100 1200 1300 1400 1500 1600 1700
Wavenumber / cm-1
Sample
(Model Catalyst)
IR Beam
QMS
NO2 Modulated
Molecular Beam
"BaAl2O4"/Al2O3
a
NO3-
"BaAl2O4"
Al2O3
NiAl(110)
Pd/"BaAl2O4"(annealed)/Al2O3
b
PdO
Pd
NO3-
NO
Pd/"BaAl2O4"/Al2O3
c
NO3-
NO2-
"BaAl2O4"/Pd/Al2O3
d
NO3-
Pd
NO2-
PdO
Increasing
Metal-Oxide
Interaction

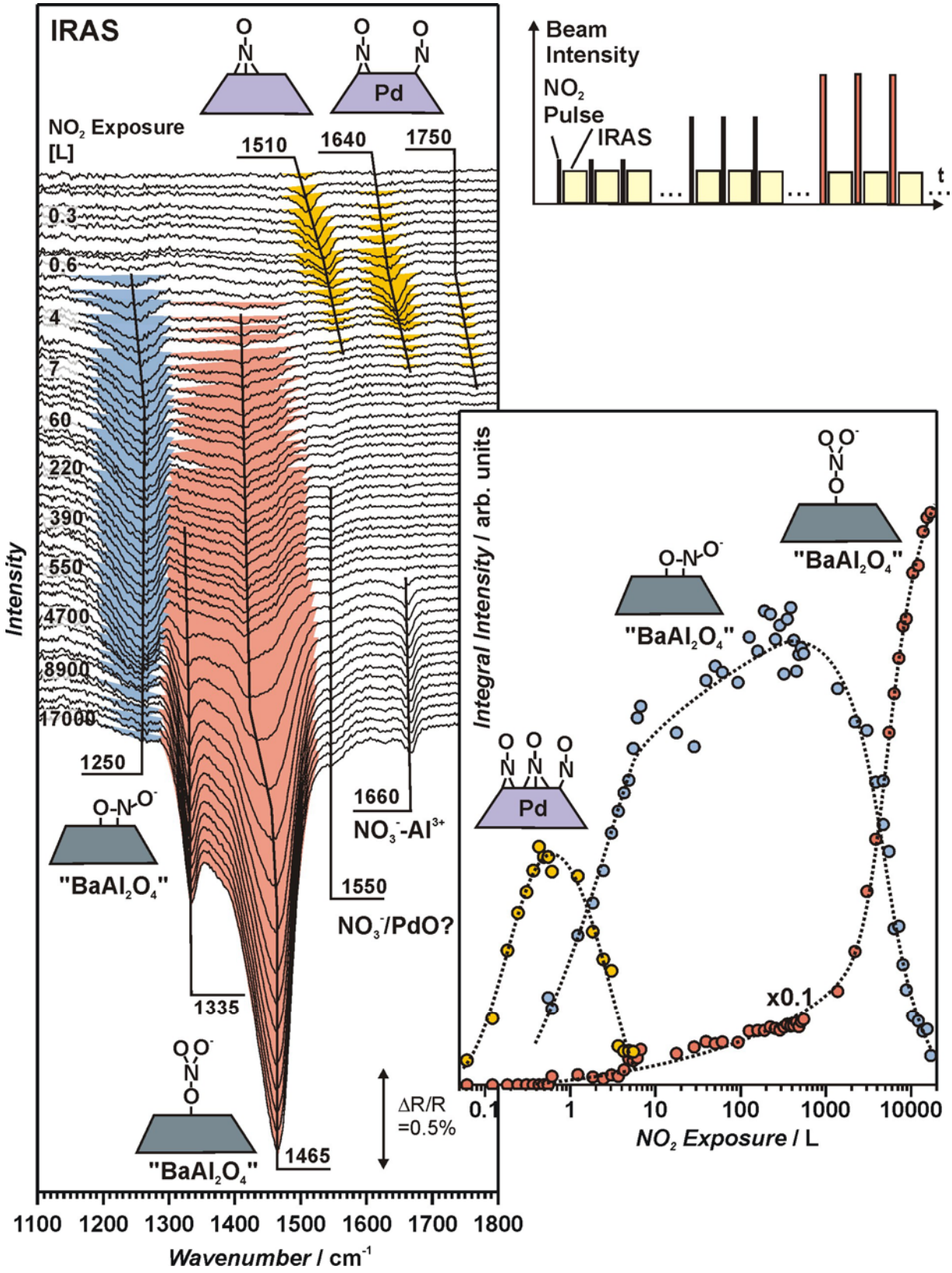
IRAS
Pd
NO2 Exposure [L]
0.3
0.6
4
7
60
220
390
550
4700
8900
17000
1510
1640
1750
1250
1660
NO3--Al3+
1550
NO3-/PdO?
1335
1465
"BaAl2O4"
ΔR/R =0.5%
Intensity
1100 1200 1300 1400 1500 1600 1700 1800
Wavenumber / cm-1
Beam Intensity
NO2 Pulse
IRAS
t
Integral Intensity / arb. units
x0.1
0.1 1 10 100 1000 10000
NO2 Exposure / L

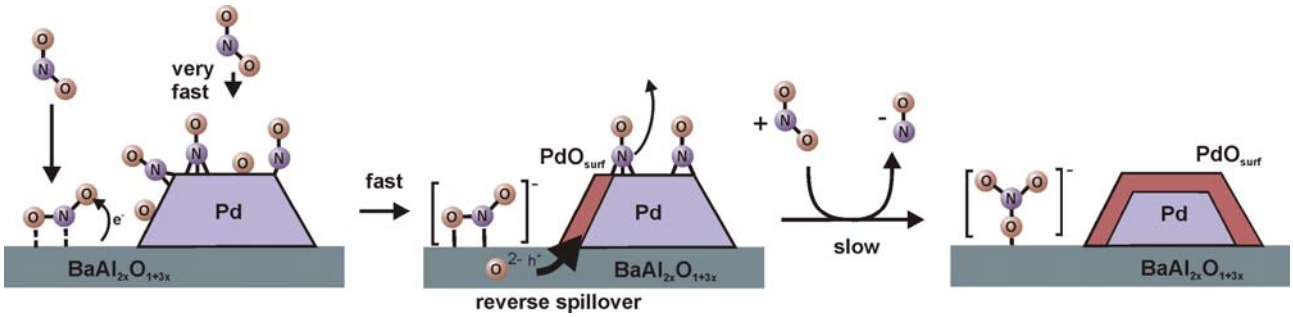
very
fast
Pd
$BaAl_{2x}O_{1+3x}$
fast
PdO_{surf}
Pd
$BaAl_{2x}O_{1+3x}$
reverse spillover
slow
PdO_{surf}
Pd
$BaAl_{2x}O_{1+3x}$